Effective Modeling of Magnetized Graphene by the Wave Concept Iterative Process Method Using Boundary Conditions

Aymen Hlali*, Zied Houaneb, and Hassen Zairi

Abstract—Due to static magnetic field, the conductivity of graphene becomes an anisotropic tensor, which complicates most modeling methodologies. A practical approach to the Wave Concept Iterative Process method (WCIP) modeling of magnetized graphene sheets as an anisotropic conductive surface from the microwave to terahertz frequencies is proposed. We first introduce a brief description of modeling magnetized graphene as an infinitesimally thin conductive sheet. Then, we present a novel manner for the implementation of the anisotropic boundary conditions using the wave concept in the WCIP method. This proposed method is benchmarked with numerical examples to demonstrate its applicability and accuracy. The proposed approach is used to compare the anisotropic model, isotropic model, and the metal for a strip waveguide. We show that the anisotropic model gives more efficient results.

1. INTRODUCTION

Magnetized graphene is an infinitesimally thin sheet biased by a magnetostatic field and behaves as an anisotropic conducting sheet characterized by a conductivity tensor [1, 2]. For the modeling of magnetized graphene, a number of numerical methods have already been developed to quantify the anisotropic properties of graphene such the method of moments (MOM) [3], finite difference time domain (FDTD) [4–6] method, and partial element equivalent circuit (PEEC) method [7].

However, each method has its advantages and drawbacks [8]. FDTD modeling of magnetized graphene has been addressed in earlier works [4–6]. In [6], an FDTD approach is developed by transforming the surface conductivity of graphene to a volumetric conductivity by dividing the thickness of graphene and implementing it by using the auxiliary differential equation (ADE) and matrix exponential method. However, this method uses volumetric discretizations, which slows the computation [4, 7, 8]. For the MOM method, it can directly implement the surface conductivity into the numerical process, but the physical process of how the magnetostatic field affects the properties of graphene is not clear since this is a purely mathematical process [7, 8].

Among these numerical methods, WCIP [9–15] has its natural advantage over any other methods. It applies the surface conductivity graphene directly without involving volumetric discretization, which significantly reduces the time consumption and memory size. In this paper, a novel model of magnetized graphene based on the wave concept is developed for the first time to analyze the anisotropy of magnetostatically biased graphene, and a comparative investigation of anisotropic and isotropic models for strip waveguide has been designed to demonstrate the effectiveness of the anisotropic model. The remainder of this paper is organized as follows. In Section 2, some theoretical aspects about the anisotropic nature of graphene are discussed, and its complex conductivity is described. Furthermore, a brief introduction to the Wave Concept Iterative Process method and formulation of the proposed

* Corresponding author: Aymen Hlali (hlaliaymen683@gmail.com).
The authors are with the Research Laboratory Smart Electricity & ICT, SEICT, National Engineering School of Carthage, University of Carthage, Tunis, Tunisia.

algorithm are detailed, including the development of the new diffraction operator of the magnetized graphene. In Section 3, numerical results are presented to demonstrate the effectiveness and accuracy of the proposed algorithm. Conclusions are made at the end of this paper.

2. THEORY AND FORMULATION

2.1. Conductivity Model of Magnetized Graphene

This section provides a brief description of graphene conductivity under a magnetic bias field for a good understanding of the following sections. Consider a graphene sheet biased with a static magnetic field perpendicular to its plane. Due to this field, graphene exhibits anisotropy [1]. Therefore, a useful technique to incorporate the magnetically biased graphene in the electromagnetic problem is to replace the graphene with an infinitesimally thin layer, defined by its anisotropic surface conductivity, expressed as [1, 2]

$$\bar{\bar{\sigma}} = \begin{pmatrix} \sigma_d & -\sigma_o \\ \sigma_o & \sigma_d \end{pmatrix} \tag{1}$$

where σ_d and σ_o are derived from the Drude model

$$\sigma_d = \sigma_{xx} = \sigma_{yy} \tag{2}$$
$$\sigma_o = \sigma_{xy} = -\sigma_{yx} \tag{3}$$

In this context, the conductivity model consists of two terms, where the former is due to the intraband conductivity and the latter to the interband conductivity [1]. However, in the low-frequency range, the interband term is negligible, and hence, the conductivity of graphene can be expressed by using the only intraband term [16, 17], whose elements are calculated through

$$\sigma_{d,intra} = -j\frac{e^2 K_B T}{\pi\hbar^2(\omega - j2\Gamma)} \left[\frac{\mu_c}{K_B T} + 2\ln\left(e^{-\frac{\mu_c}{K_B T}} + 1\right) \right] \tag{4}$$

and

$$\sigma_{o,intra} = -\frac{e^2 V_F^2 eB}{\pi\hbar^2(\omega - j2\Gamma)^2} \left[1 - 2\left(e^{-\frac{\mu_c}{K_B T}} + 1\right)^{-1} \right] \tag{5}$$

where K_B is the Boltzmann constant, $\hbar$ the reduced Planck's constant, e the electron charge, ω the angular frequency, Γ the scattering rate, T the temperature, V_F the Fermi velocity, B the amplitude of the static magnetic field bias, and μ_c the chemical potential.

2.2. Formulation of WCIP Method

Analysis of planar structures with our electromagnetic method called wave concept iterative method WCIP has been explained in detail in different published articles [9–15]. Therefore, in this subsection, a brief overview of the WCIP method is presented. This method is based on the Wave Concept, which is introduced by writing the tangential electric field $\vec{E}_i$ and a surface tangential current density $\vec{J}_i$ in terms of incident and reflected waves (see Fig. 1). It leads to the following set of equations [9–15]

$$\vec{A}_i = \frac{1}{2\sqrt{Z_{0i}}}(\vec{E}_i + Z_{0i}\vec{J}_i) \tag{6}$$

$$\vec{B}_i = \frac{1}{2\sqrt{Z_{0i}}}(\vec{E}_i - Z_{0i}\vec{J}_i) \tag{7}$$

where $\vec{B}_i$ and $\vec{A}_i$ are the incident and reflected waves associated with the discontinuity interface. Z_{0i} is the characteristic impedance of the middle i ($i = 1, 2$) given by $Z_{0i} = \sqrt{\frac{\mu_0}{\varepsilon_0\varepsilon_{ri}}}$ where ε_{ri} is the relative permittivity of the region i. $\vec{J}_i$ is the surface tangential current density which defines $\vec{J}_i = \vec{H}_i \times \vec{n}_i$ with $\vec{n}_i$ as the unit vector normal to the surface, and $\vec{E}_i$ and $\vec{H}_i$ are the tangential electric and magnetic

fields, respectively. After process convergence, the scattering matrix S_{ij} can be obtained by the following equation

$$[S] = \frac{1 - [Y]}{1 + [Y]} \tag{8}$$

where $[Y]$ is the matrix admittance. A schematic description of the WCIP algorithm is illustrated in Fig. 2.
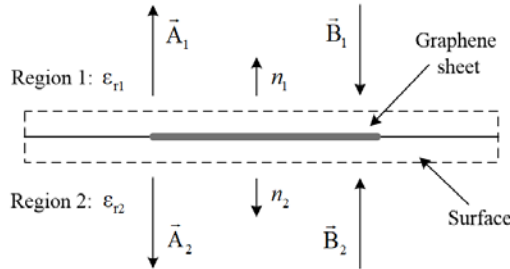
Figure 1. Incident and reflected waves on both sides of the interface.
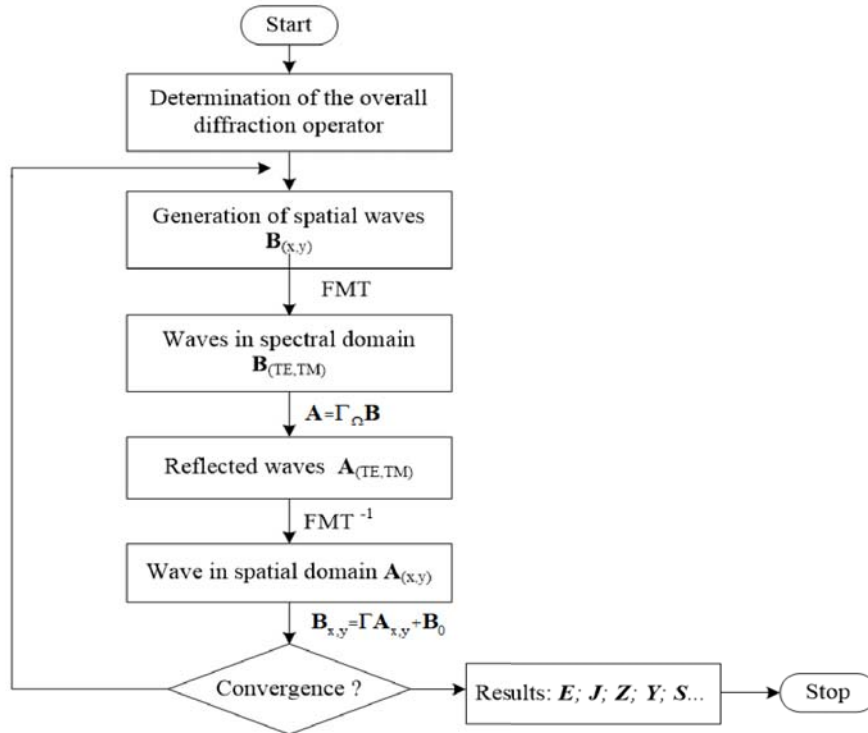
Figure 2. Schematic description of the WCIP algorithm.

2.3. Implementation of the Anisotropic Boundary Conditions of Graphene in the WCIP Method

Graphene is introduced in the WCIP method as boundary condition via the surface current and electric field using surface conductivity $\bar{\bar{\sigma}}$. The electromagnetic boundary condition at the magnetized graphene sheet can be written as [1]

$$\vec{n} \times (\vec{H}_1 - \vec{H}_2) = \vec{J}_s \tag{9a}$$

$$= \bar{\bar{\sigma}} \vec{E} \tag{9b}$$

where $\vec{n}$ denotes the unit vector normal to the graphene sheet; $\vec{H}_1$ and $\vec{H}_2$ are the magnetic fields at two sides of the sheet; $\vec{J}_s$ is the surface current density; and $\vec{E}$ is the electric field.

To incorporate the graphene sheet into the WCIP method, we consider a graphene sheet positioned parallel to the xy plane and biased by a magnetostatic field, directed in the z direction. An equivalent model of magnetized graphene sheet in the WCIP method is illustrated in Fig. 3.
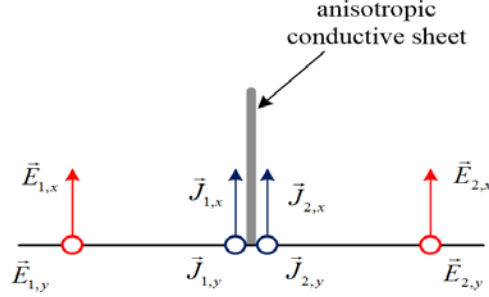
Figure 3. Equivalent model of magnetized graphene sheet in the WCIP method.

Substituting Eq. (1) in Eq. (9) and decomposing the equation, the surface current density becomes

$$\vec{J}_x = \sigma_d \vec{E}_x - \sigma_o \vec{E}_y \tag{10}$$

$$\vec{J}_y = \sigma_o \vec{E}_x + \sigma_d \vec{E}_y \tag{11}$$

Now, the primary issue is to define the connection between the surface currents $\vec{J}_x$, $\vec{J}_y$ and the electric fields $\vec{E}_x$, $\vec{E}_y$ for the two sides of the sheet $\vec{J}_{1,x}$, $\vec{J}_{2,x}$; $\vec{J}_{1,y}$, $\vec{J}_{2,y}$ and $\vec{E}_{1,x}$, $\vec{E}_{2,x}$; $\vec{E}_{1,y}$, $\vec{E}_{2,y}$, respectively. Since the source is bilateral, the component of the surface current and electric field can be written as

$$\vec{J}_x = \vec{J}_{1,x} + \vec{J}_{2,x} \tag{12}$$

$$\vec{J}_y = \vec{J}_{1,y} + \vec{J}_{2,y} \tag{13}$$

and

$$\vec{E}_x = \vec{E}_{1,x} = \vec{E}_{2,x} \tag{14}$$

$$\vec{E}_y = \vec{E}_{1,y} = \vec{E}_{2,y} \tag{15}$$

By replacing Equations (12), (13), (14) and (15) in Equations (10) and (11), we obtain the following equations

$$\vec{J}_{1,x} + \vec{J}_{2,x} = \sigma_d \vec{E}_{i,x} - \sigma_o \vec{E}_{i,y} \tag{16}$$

$$\vec{J}_{1,y} + \vec{J}_{2,y} = \sigma_o \vec{E}_{i,x} + \sigma_d \vec{E}_{i,y} \tag{17}$$

where $\vec{E}_{i,x}$ and $\vec{E}_{i,y}$ are the components of $\vec{E}_{1,x}$, $\vec{E}_{2,x}$, $\vec{E}_{1,y}$ and $\vec{E}_{2,y}$, respectively.

However, the incorporation of boundary conditions in the WCIP method is enforced by redefining the surface current and electric field in terms of waves. Therefore, Equations (16) and (17) can be rewritten as

$$\frac{1}{\sqrt{Z_{01}}}(\vec{A}_{1,x} - \vec{B}_{1,x}) + \frac{1}{\sqrt{Z_{02}}}(\vec{A}_{2,x} - \vec{B}_{2,x}) = \sigma_d \sqrt{Z_{01}}(\vec{A}_{1,x} + \vec{B}_{1,x}) - \sigma_o \sqrt{Z_{01}}(\vec{A}_{1,y} + \vec{B}_{1,y}) \tag{18}$$

$$\frac{1}{\sqrt{Z_{01}}}(\vec{A}_{1,x} - \vec{B}_{1,x}) + \frac{1}{\sqrt{Z_{02}}}(\vec{A}_{2,x} - \vec{B}_{2,x}) = \sigma_d \sqrt{Z_{02}}(\vec{A}_{2,x} + \vec{B}_{2,x}) - \sigma_o \sqrt{Z_{02}}(\vec{A}_{2,y} + \vec{B}_{2,y}) \tag{19}$$

$$\frac{1}{\sqrt{Z_{01}}}(\vec{A}_{1,y} - \vec{B}_{1,y}) + \frac{1}{\sqrt{Z_{02}}}(\vec{A}_{2,y} - \vec{B}_{2,y}) = \sigma_d \sqrt{Z_{01}}(\vec{A}_{1,y} + \vec{B}_{1,y}) + \sigma_o \sqrt{Z_{01}}(\vec{A}_{1,x} + \vec{B}_{1,x}) \tag{20}$$

$$\frac{1}{\sqrt{Z_{01}}}(\vec{A}_{1,y} - \vec{B}_{1,y}) + \frac{1}{\sqrt{Z_{02}}}(\vec{A}_{2,y} - \vec{B}_{2,y}) = \sigma_d \sqrt{Z_{02}}(\vec{A}_{2,y} + \vec{B}_{2,y}) + \sigma_o \sqrt{Z_{02}}(\vec{A}_{2,x} + \vec{B}_{2,x}) \tag{21}$$

The resolution of these equations requires the introduction of other hypotheses. According to the relations given by Equations (14) and (15), it is possible to obtain

$$\vec{B}_{1,x} = \frac{\sqrt{Z_2}}{\sqrt{Z_1}}(\vec{A}_{2,x} + \vec{B}_{2,x}) - \vec{A}_{1,x} \tag{22}$$

$$\vec{B}_{1,y} = \frac{\sqrt{Z_2}}{\sqrt{Z_1}}(\vec{A}_{2,y} + \vec{B}_{2,y}) - \vec{A}_{1,y} \tag{23}$$

$$\vec{B}_{2,x} = \frac{\sqrt{Z_1}}{\sqrt{Z_2}}(\vec{A}_{1,x} + \vec{B}_{1,x}) - \vec{A}_{2,x} \tag{24}$$

$$\vec{B}_{2,y} = \frac{\sqrt{Z_1}}{\sqrt{Z_2}}(\vec{A}_{1,y} + \vec{B}_{1,y}) - \vec{A}_{2,y} \tag{25}$$

After a mathematical resolution among Equations (18), (19), (20), (21), (22), (23), (24) and (25) by calculating the relationship between normalized incident and reflected waves, we can derive the scattering matrix of graphene as

$$\begin{pmatrix} \vec{B}_{1,x} \\ \vec{B}_{1,y} \\ \vec{B}_{2,x} \\ \vec{B}_{2,y} \end{pmatrix} = \begin{pmatrix} S_{11} & S_{12} & S_{13} & S_{14} \\ S_{21} & S_{22} & S_{23} & S_{24} \\ S_{31} & S_{32} & S_{33} & S_{34} \\ S_{41} & S_{42} & S_{43} & S_{44} \end{pmatrix} \begin{pmatrix} \vec{A}_{1,x} \\ \vec{A}_{1,y} \\ \vec{A}_{2,x} \\ \vec{A}_{2,y} \end{pmatrix} \tag{26}$$

where S_{ij} are defined by

$$S_{11} = \frac{X_4 X_1 - X_2^2}{X_1^2 + X_2^2}; \quad S_{12} = \frac{X_4 X_2}{X_1^2 + X_2^2}$$

$$S_{13} = \frac{2X_1(Z_{02}\sqrt{Z}_{01})}{X_1^2 + X_2^2}; \quad S_{14} = \frac{2\sigma_o\sqrt{Z}_{01}(Z_{02}\sqrt{Z}_{01})^2}{X_1^2 + X_2^2}$$

$$S_{21} = \frac{-2\sigma_o(Z_{02}\sqrt{Z}_{01})^2}{X_1^2 + X_2^2}; \quad S_{22} = S_{11}$$

$$S_{23} = \frac{-2\sigma_o(Z_{02}\sqrt{Z}_{01})^2}{\sqrt{Z}_{02}[X_1^2 + X_2^2]}; \quad S_{24} = \frac{2X_1(Z_{02}\sqrt{Z}_{01})}{\sqrt{Z}_{02}[X_1^2 + X_2^2]}$$

$$S_{31} = \frac{2X_1(Z_{01}\sqrt{Z}_{02})}{\sqrt{Z}_{01}[X_1^2 + X_3^2]}; \quad S_{32} = \frac{2\sigma_o(Z_{01}\sqrt{Z}_{02})^2}{X_1^2 + X_3^2}$$

$$S_{33} = \frac{X_5 X_1 - X_3^2}{X_1^2 + X_3^2}; \quad S_{34} = S_{32}$$

$$S_{41} = \frac{-2\sigma_o\sqrt{Z}_{02}(Z_{01}\sqrt{Z}_{02})^2}{\sqrt{Z}_{01}(X_1^2 - X_3^2)}; \quad S_{42} = \frac{2X_1(Z_{01}\sqrt{Z}_{02})}{\sqrt{Z}_{01}(X_1^2 - X_3^2)}$$

$$S_{43} = \frac{-2\sigma_o(Z_{01}\sqrt{Z}_{02})^2}{X_1^2 - X_3^2}; \quad S_{44} = \frac{X_5 X_1 - X_3^2}{X_1^2 - X_3^2}$$

and

$$X_1 = Z_{02} + Z_{01} + \sigma_d Z_{01} Z_{02} \tag{27}$$

$$X_2 = (\sigma_o\sqrt{Z}_{01})(Z_{02}\sqrt{Z}_{01}) \tag{28}$$

$$X_3 = (\sigma_o\sqrt{Z}_{02})(Z_{01}\sqrt{Z}_{02}) \tag{29}$$

$$X_4 = Z_{02} - Z_{01} - \sigma_d Z_{01} Z_{02} \tag{30}$$

$$X_5 = Z_{01} - Z_{02} - \sigma_d Z_{01} Z_{02} \tag{31}$$

2.4. Determination of the New Diffraction Operator for Anisotropic Media

In order to establish the total diffraction operator, it is necessary to determine the relationship between incident and reflected waves with the anisotropic form while retaining the isotropy of the source and dielectric domains. In the isotropic formulation, the relations between the reflected and incident waves in the source and dielectric domains are written as follows [9–15]

$$\vec{B}_1 = S_{11}\vec{A}_1 + S_{12}\vec{A}_2 \tag{32}$$

$$\vec{B}_2 = S_{21}\vec{A}_1 + S_{22}\vec{A}_2 \tag{33}$$

In the anisotropic formulation, these relationships take the following matrix form

$$\begin{pmatrix} \vec{B}_{1,x} \\ \vec{B}_{1,y} \\ \vec{B}_{2,x} \\ \vec{B}_{2,y} \end{pmatrix} = \begin{pmatrix} S_{11,x} & 0 & S_{12,x} & 0 \\ 0 & S_{11,y} & 0 & S_{12,y} \\ S_{21,x} & 0 & S_{22,x} & 0 \\ 0 & S_{21,y} & 0 & S_{22,y} \end{pmatrix} \begin{pmatrix} \vec{A}_{1,x} \\ \vec{A}_{1,y} \\ \vec{A}_{2,x} \\ \vec{A}_{2,y} \end{pmatrix} \tag{34}$$

where

$$S_{11} = S_{11,x} = S_{11,y} \tag{35}$$

$$S_{12} = S_{12,x} = S_{12,y} \tag{36}$$

$$S_{21} = S_{21,x} = S_{21,y} \tag{37}$$

$$S_{22} = S_{22,x} = S_{22,y} \tag{38}$$

Modeling with the WCIP method requires the meshing of the interface surface into small sub-domains. The graphene, metal, dielectric and source domains are characterized by the corresponding matrix H_g, H_m, H_d and H_s. The domain-matrix elements take value 1 in the corresponding cells and zero elsewhere. However, we can express boundary conditions in terms of waves in each region. The diffraction operator of the source, dielectric and metal domains are described in [9–15]. Finally, it is possible to determine the overall diffraction operator. From that, the overall diffraction operator can be obtained by the following equation

$$\Gamma = \Gamma_G + \Gamma_m + \Gamma_d + \Gamma_s = \begin{pmatrix} \Gamma_{11} & \Gamma_{12} & \Gamma_{13} & \Gamma_{14} \\ \Gamma_{21} & \Gamma_{22} & \Gamma_{23} & \Gamma_{24} \\ \Gamma_{31} & \Gamma_{32} & \Gamma_{33} & \Gamma_{34} \\ \Gamma_{41} & \Gamma_{42} & \Gamma_{43} & \Gamma_{44} \end{pmatrix} \tag{39}$$

where $\Gamma_G, \Gamma_m, \Gamma_d$ and Γ_s are respectively the graphene, metal, dielectric and source domain diffraction operators.

3. NUMERICAL RESULTS AND DISCUSSION

3.1. Algorithm Verification

To validate and demonstrate the accuracy of this proposed algorithm, the total transmission coefficient, the Faraday rotation angle, and the cross-polarized transmission coefficient of an infinite graphene sheet are studied by comparing the analytical solution to the extracted results from the proposed method.

The first simulation focuses on the surface conductivity σ_d and σ_o of a graphene sheet. Graphene parameters are selected as $\tau = 0.1\,\mathrm{ps}$, $T = 300\,\mathrm{K}$, while magnetic field intensity B and chemical potentials μ_c vary from 5 to 50 T and 0.1 to 0.4 eV, respectively. The real and imaginary parts are shown in Fig. 4.

At low frequencies, we can see from these figures the effect of changing μ_c and B on the conductivity; the conductivity increases with their increasing [18].

A second example is considered to compare the analytical estimations to the numerically extracted results from the proposed method. Graphene parameters are selected as $\mu_c = 0.117\,\mathrm{eV}$ and $\tau = 0.117\,\mathrm{ps}$ (extracted from the typical graphene values of mobility $\mu = 10000\,\mathrm{cm^2/(Vs)}$ and carrier density
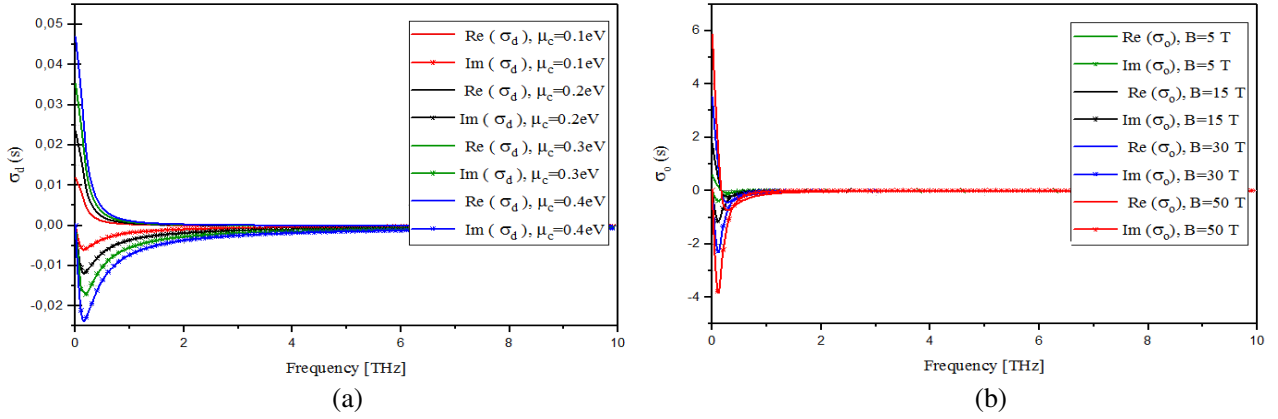
Figure 4. Real and imaginary parts of the surface conductivity: (a) σ_d for different chemical potentials μ_c, and (b) σ_o for different biasing magnetostatic fields B.
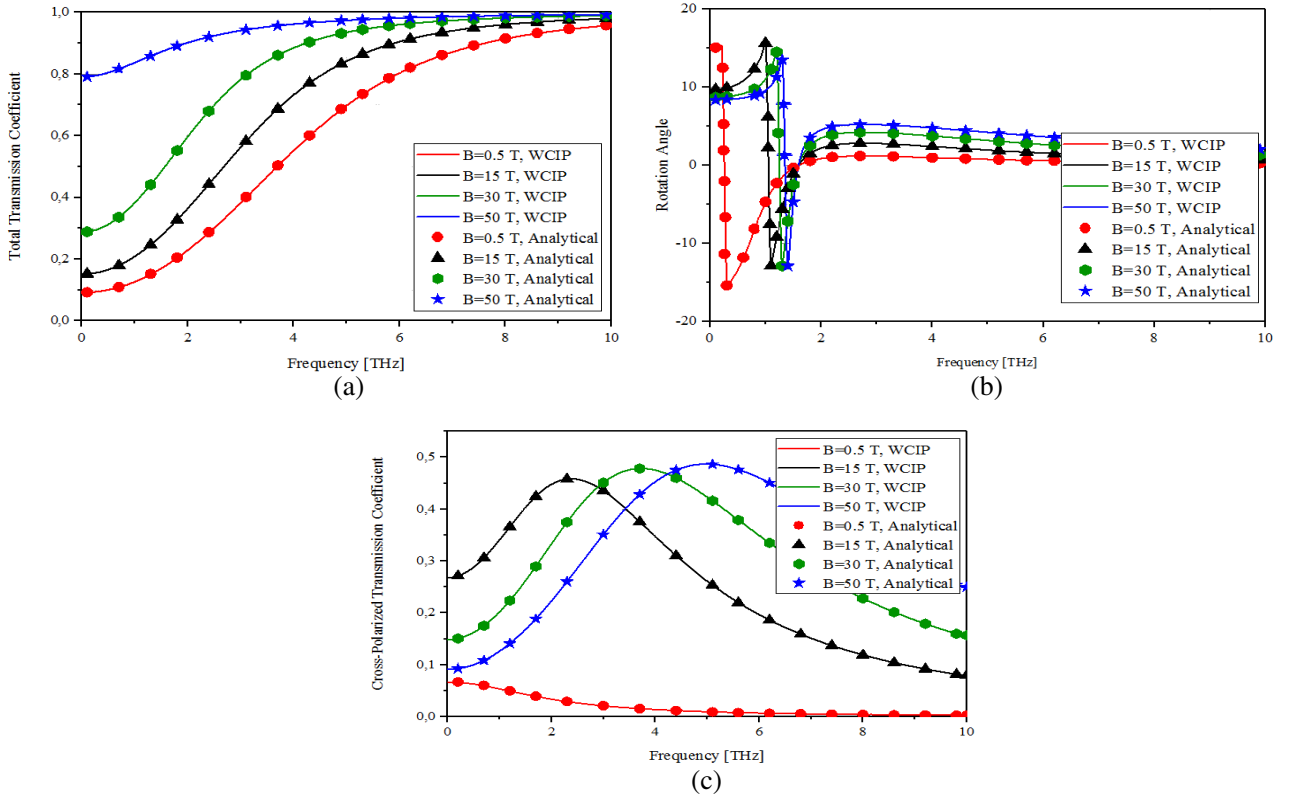
Figure 5. (a) The total transmission coefficients, (b) Faraday rotation angle, and (c) the cross-polarized transmission coefficients of the graphene sheet versus frequency for different magnetic field values.

$n_s = 10^{12} \, \text{cm}^{-2}$) at room's temperature $T = 300 \, \text{K}$, while magnetic field intensity B varies from 0.5 to 50 T. In Fig. 5, the total transmission coefficient [6, 16, 19]

$$T_{tot,ana} = \frac{2\sqrt{|2 + \sigma_d \eta_o|^2 + |\sigma_o \eta_o|^2}}{|2 + \sigma_d \eta_o|^2 + |\sigma_o \eta_o|^2} \tag{40}$$

the Faraday rotation angle

$$\theta_{F,ana} = \tan^{-1}\left(\frac{\eta_o \sigma_o}{2 + \eta_o \sigma_d}\right) \tag{41}$$

and the cross-polarized transmission coefficient

$$T_{cross,ana} = \frac{2\left|\eta_o \sigma_o\right|}{\left|(2 + \eta_o \sigma_d)^2 + (\eta_o \sigma_o)^2\right|} \tag{42}$$

are also provided with different biasing magnetostatic fields, where η_o is the EM wave impedance in free space.

Outstanding agreements between the numerical results and analytical ones are observed at an extensive frequency range; this numerically validates our proposed method. The results show that the magnetostatic biasing has significant impacts on the electromagnetic waves propagating through a graphene sheet.

3.2. Comparative Investigation of Anisotropic and Isotropic Models for Strip Waveguide

A third example is considered to compare the anisotropic model and isotropic model for response of the strip waveguide. The formulation developed in the previous section was implemented in FORTRAN code. The proposed strip waveguide is shown in Fig. 6. The simulation setup consists of the graphene waveguide printed on a Teflon substrate with dielectric constant of $\varepsilon_r = 2.8$ which is normally illuminated by an x-polarized plane wave. The graphene waveguide is located in the xy-plane and biased by a static magnetic field, B, along the z-direction. The length and width of the substrate are kept fixed at $105\,\mu$m and $105\,\mu$m, respectively, whereas the height of the substrate is fixed at $3\,\mu$m. The width of the graphene strip is assumed to be $11.484\,\mu$m. A grid of 128 by 128 pixels is used to define the interface with extreme fidelity to the geometric parameters. Other graphene parameters are given by $\mu_c = 0.117\,$eV and $\tau = 0.117\,$ps, at room temperature $T = 300\,$K, while magnetic field intensity B is $0.5\,$T.
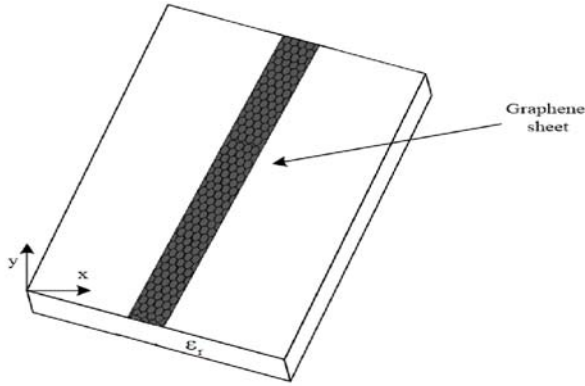
Figure 6. Schematic of the proposed strip waveguide.
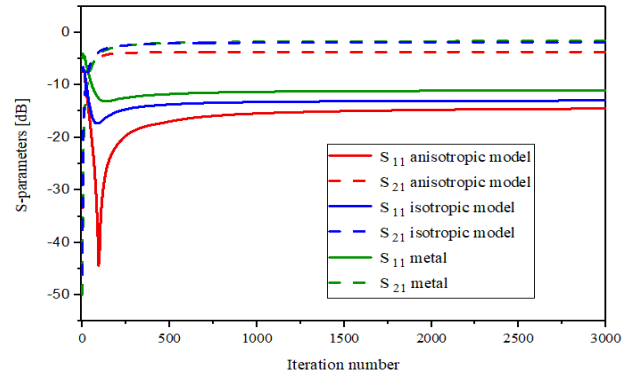
Figure 7. Convergence of the s-parameters versus the number of iterations.

In order to compare the performance of an anisotropic and isotropic model of graphene in the terahertz region, we started with the convergence study and boundary conditions. Fig. 7 shows the variation of s-parameters as a function of the number of iterations at resonant frequencies.

We find that the convergence with the anisotropic model is obtained from 1400 iterations, 900 iterations with the isotropic model and 800 iterations for the metal. Figs. 8 and 9 illustrate the distribution of currents and fields for the structure.

According to these figures, we notice that the electric field and current density satisfy the boundary conditions, since the density of the current is defined only on the graphene and metal, and zero on the dielectric. The electric field is zero on graphene and metal, and different from zero on the dielectric.

Fig. 10 illustrates the variation of the reflection coefficient and transmission coefficient for the three configurations, namely, the anisotropic model, isotropic model, and metal.
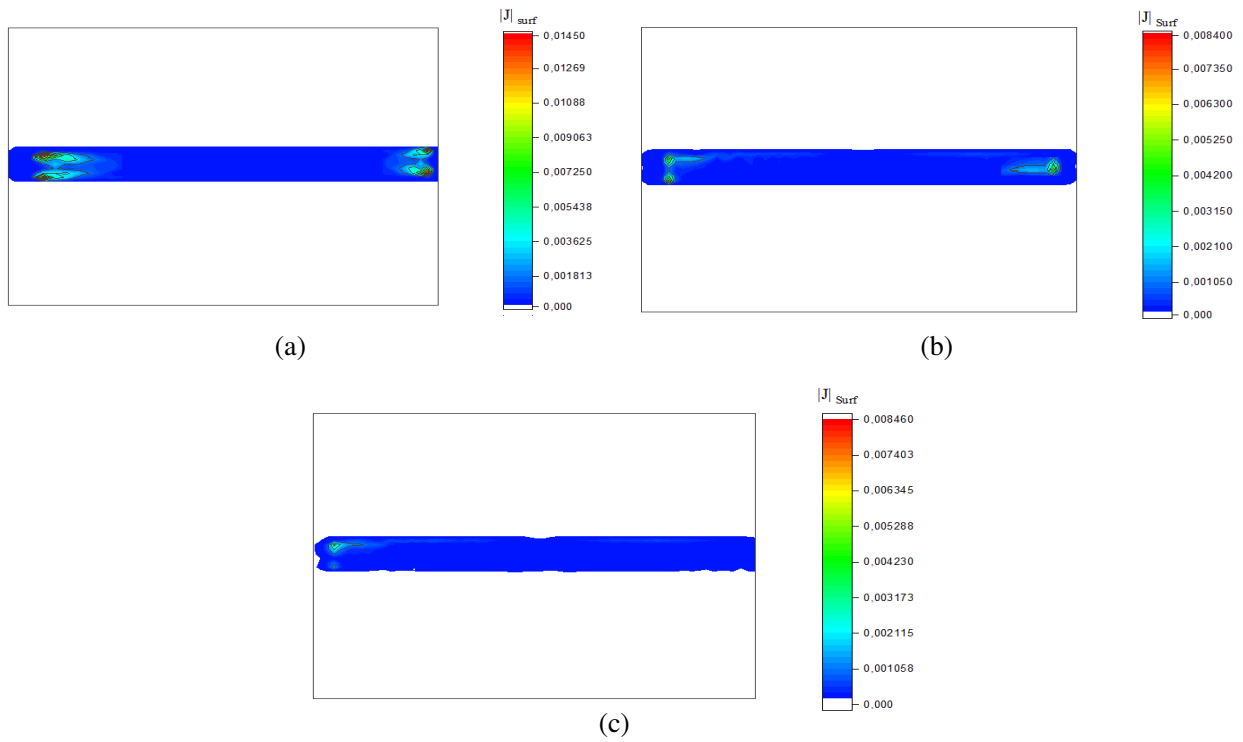
Figure 8. Distribution of the current density of the interface for the three configurations: (a) anisotropic model, (b) isotropic model, and (c) metal.
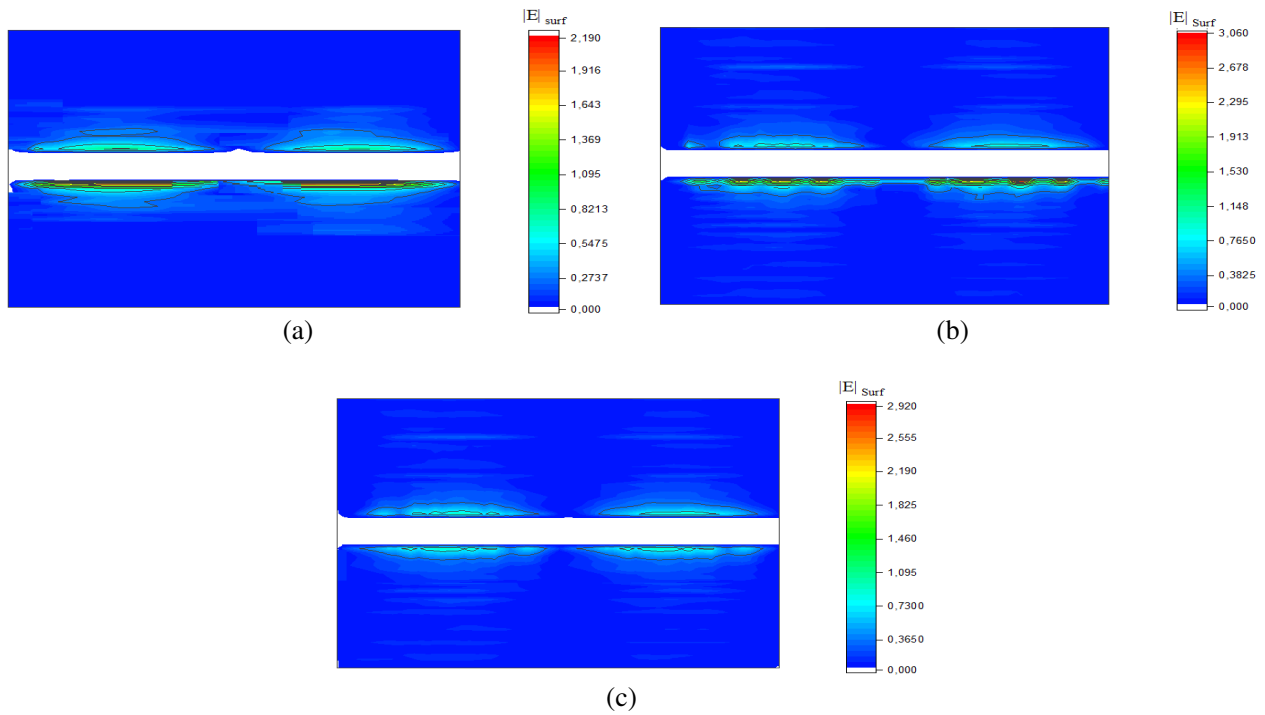
Figure 9. Distribution of the electric field of the interface for the three configurations: (a) anisotropic model, (b) isotropic model, and (c) metal.
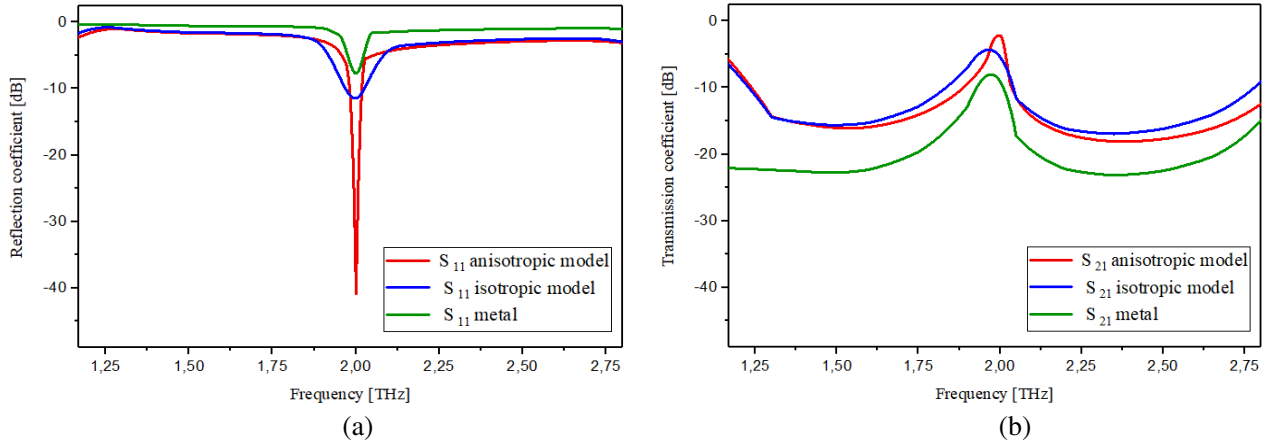
Figure 10. Comparison of simulated results: (a) Reflection coefficient, and (b) transmission coefficient.
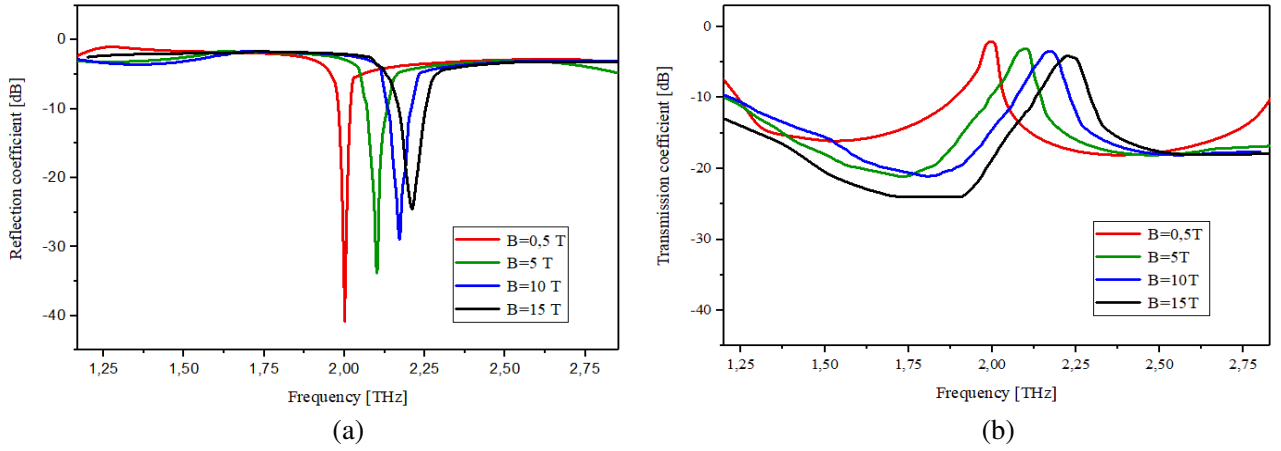
Figure 11. Simulated results of the anisotropic model for different magnetic fields: (a) Reflection coefficient, and (b) Transmission coefficient.

It is shown that the reflection coefficient of the metal-based waveguide is wrongly adapted, and it is evident, since the metal is not usable in the THz regime. Besides that, with the isotropic model of graphene, the waveguide performance is enhanced drastically compared to the metal-based waveguide in terms of the reflection coefficient. In this case, the return loss is reduced from -8 to -13 dB. But the anisotropic model showed better adaptation. So, the anisotropic model gives better and more efficient results than the isotropic model for waveguide applications [20].

The simulation results obtained for S-parameters characteristics over the considered 0.5–15 T range of magnetic field intensity are shown in Fig. 11. The tunability of resonance frequency f_r with changing of the magnetic field can be seen. It is recognized that as magnetic field increases from 0.05 to 15 T, the value of f_r is increased from 2.001 to 2.2109 THz. It is exciting to note that the return loss is increased by increasing the magnetic field intensity.

4. CONCLUSION

In this paper, a novel WCIP based algorithm is developed to model a magnetized graphene sheet using an anisotropic surface boundary condition. The effectiveness of the proposed algorithm is verified by studying the total transmission coefficient, Faraday rotation angle, and cross-polarized transmission coefficient of an infinite graphene sheet, and by comparing the analytical solution to the extracted results

from the proposed method. The main advantage over the earlier approaches which consider graphene sheet as a volumetric layer is that the proposed plan directly implements the surface conductivity into the numerical process without involving volumetric discretization, which significantly reduces the time consumption and memory size. A second example was supported to compare the anisotropic model and isotropic model for the waveguide to demonstrate the effectiveness of the anisotropic model for waveguide applications.

REFERENCES

1. Hanson, G. W., "Dyadic Green's functions for an anisotropic, non-local model of biased graphene," *IEEE Transactions on Antennas and Propagation*, Vol. 103, 747–757, 2008.
2. Lovat, G., "Equivalent circuit for electromagnetic interaction and transmission through graphene sheets," *IEEE Transactions on Electromagnetic*, Vol. 54, 101–109, 2012.
3. Tamagnone, M., A. Fallahi, J. R. Mosig, and J. Perruisseau-Carrier, "Fundamental limits and near-optimal design of graphene modulators and non-reciprocal devices," *Nature Photonics*, 556–563, 2014.
4. Feizi, M., V. Nayyeri, and O. M. Ramahi, "Modeling magnetized graphene in thefinite-difference time-domain method using an anisotropic surface boundary condition," *IEEE Transactions on Antennas and Propagation*, Vol. 66, 233–241, 2018.
5. Amanatiadis, S. A., N. V. Kantartzis, T. Ohtani, and Y. Kanai, "Precise modeling of magnetically-biased graphene through a recursive convolutional FDTD method," *IEEE Transactions on Magnetics*, Vol. 54, 233–241, 2018.
6. Wang, X.-H., W.-Y. Yin, and Z. Chen, "Matrix exponential FDTD modeling of magnetized graphene sheet," *IEEE Antennas and Wireless Propagation Letters*, Vol. 12, 1129–1132, 2013.
7. Cao, Y. S., P. Li, L. J. Jiang, and A. E. Ruehli, "The derived equivalent circuit model for magnetized anisotropic graphene," *IEEE Antennas and Wireless Propagation Letters*, Vol. 65, 948–953, 2017.
8. Shao, Y., J. J. Yang, and M. Huang, "A review of computational electromagnetic methods for graphene modeling," *International Journal of Antennas and Propagation*, Vol. 81, 1–6, 2016.
9. Azizi, M., M. Boussouis, H. Aubert, and H. Baudrand, "A three-dimensional analysis of planar discontinuities by an iterative method," *Microwave and Optical Technology Letters*, Vol. 13, 372–376, 1996.
10. Gharsallah, A., A. Gharbi, and H. Baudrand, "Efficient analysis of multiport passive circuits using the iterative technique," *Electromagnetics*, Vol. 81, 73–84, 2001.
11. Zairi, H., A. Gharsallah, A. Gharbi, and H. Baudrand, "A new iterative method for analysing nonlinear photonic-crystal structures," *International Journal of Electronics*, Vol. 97, 1329–1337, 2010.
12. Mami, A., H. Zairi, A. Gharsallah, and H. Baudrand, "Analysis of microwave components and circuits using the iterative method," *International Journal of RF and Microwave*, Vol. 81, 404–414, 2004.
13. Tellache, M., Y. Lamhene, B. Haraoubia, and H. Baudrand, "Application of wave concept iterative process to analyse microwave planar circuits," *International Journal of Applied Electromagnetics and Mechanics*, Vol. 29, 131–143, 2009.
14. Houaneb, Z., H. Zairi, A. Gharsallah, and H. Baudrand, "A newwave concept iterative method in cylindrical coordinates for modeling of circular planar circuits," *Eighth Inter. Multi-Conference on Systems, Signals Devices.*, 1–7, 2011.
15. Zairi, H., A. Gharsallah, A. Gharbi, and H. Baudrand, "Analysis of planar circuits using a multigrid iterative method," *IEE Proc. Micro., Antennas and Prop.*, Vol. 153, 109–162, 2006.
16. Li, P. and L. J. Jiang, "Modeling of magnetized graphene from microwave to THz range by DGTD with a scalar RBC and an ADE," *IEEE Transactions on Antennas and Propagation*, Vol. 63, 4458–4467, 2015.

17. Shapoval, O. V., J. S. Gomez-Diaz, J. Perruisseau-Carrier, J. R. Mosig, and A. I. Nosich, "Integral equation analysis of plane wave scattering by coplanar graphene-strip gratings in the THz range," *IEEE Transactions on Terahertz Science and Technology*, Vol. 3, 666–674, 2013.

18. Guo, Y., T. Zhang, W.-Y. Yin, and X.-H. Wang, "Improved hybrid FDTD method for studying tunable graphene frequency-selective surfaces (GFSS) for THz-wave applications," *IEEE Transactions on Terahertz Science and Technology*, Vol. 5, 358–367, 2015.

19. Sounas, D. L. and C. Caloz, "Gyrotropy and nonreciprocity of graphene for microwave applications," *IEEE Transactions on Microwave Theory and Techniques*, Vol. 60, 901–914, 2012.

20. Chang, Z. and K. S. chiang, "Experimental verification of optical models of graphene with multimode slab waveguides," *Optics Letters*, Vol. 4, 2130–2134, 2016.